

**IMMOBILIZATION OF RADIONUCLIDES IN THE HANFORD VADOSE ZONE BY INCORPORATION IN  
SOLID PHASES**

**Project: DE-FG07-99ER15010**

**Samuel J. Traina<sup>1</sup>**

**Sierra Nevada Research Insititue  
University of California, Merced  
Merced, CA 95344**

**Final Project Report**

<sup>1</sup>Formerly of The Ohio State University

## TABLE OF CONTENTS

1. Homo- and heterogeneous reactions of Cr(VI) with simulated high level waste fluids, specimen minerals and Hanford sediments.....	3
2. Precipitation and adsorption of uranium in highly alkaline solutions: possible chemical reactions occurring in the Hanford vadose zone beneath the tank farm. ....	12
3. Research Products.....	26

# HOMO- AND HETEROGENEOUS REACTIONS OF Cr(VI) WITH SIMULATED HIGH LEVEL WASTE FLUIDS, SPECIMEN MINERALS AND HANFORD SEDIMENTS.

## Cr(VI) reduction reactions.

The objective of this study was to examine the homogeneous and heterogeneous reduction of Cr(VI) by dissolved Fe(II) and Fe(II)-containing minerals under conditions thought to be indicative of HLW fluids (high pH, high ionic strength and high temperature). Many investigators have reported the homogeneous reduction of Cr(VI) by dissolved Fe(II), but less information is available for pH values > 8. The first part of this effort evaluated the ability of dissolved Fe(II) to reduce dissolved Cr(VI) in hyperalkaline solutions.

### A. Homogeneous reduction experiments.

Homogeneous reduction of Cr(VI) by dissolved Fe(II) was examined at 50°C and 25°C in the presence and absence of  $\text{CO}_3^{2-}$  and  $\text{O}_2$ . The latter conditions were established by the use of deoxygenated solutions in an Ar(g)-filled glove box. All experiments were conducted in the presence of 1 mol L<sup>-1</sup> NaOH. The initial concentration of dissolved Fe(II) ranged from 0 to 3 mmol L<sup>-1</sup> (as FeCl<sub>2</sub>), dissolved Cr(VI) (as Na<sub>2</sub>CrO<sub>4</sub>) was 1 mmol L<sup>-1</sup>. Some experiments were conducted in the presence of 1 mol L<sup>-1</sup> NaNO<sub>3</sub> and 1 or 10 mmol L<sup>-1</sup> Na<sub>2</sub>CO<sub>3</sub>, to examine the respective effects of NO<sub>3</sub><sup>-</sup> and CO<sub>3</sub><sup>2-</sup> on Cr(VI) reduction. In all cases, addition of Na<sub>2</sub>CrO<sub>4</sub> to

FeCl<sub>2</sub> solutions induced virtually instantaneous formation of dark, reddish brown precipitates and removal of Cr from solution (Fig. 1). No precipitates were observed for the first 2 days of reaction in Fe(II) solutions in the absence of dissolved Cr(VI), or for the entire reaction period (1 week) in Cr(VI) solutions lacking dissolved Fe(II). Colorimetric analyses indicated all dissolved Cr was Cr(VI). Patterson and Fendorf [1] found that at pH 8.5 to 10.5, Cr was not longer from solution once a red-brown precipitate (as of Fe(III)hydroxide) had formed. Eary and Rai [2] suggested that at pH > 10, chromate is less efficiently reduced by ferrous ions as evidenced by nonstoichiometric reduction.

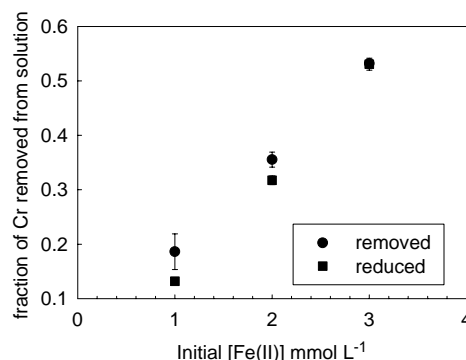


Figure 1. Removal of Cr from solution upon reaction with dissolved Fe(II), in 1 mol L<sup>-1</sup> NaOH.

Buerge and Hug [3] described the formation of x-ray amorphous precipitates with a composition of Fe<sub>0.75</sub>Cr<sub>0.25</sub>(OH)<sub>3</sub>(s). In the present study, SEM images of the precipitates showed small particles < 1 μm in cross-section. Energy dispersive x-ray analyses of the solids indicated average Fe:Cr ratios of 3.17 and 2.84 for initial Fe:Cr solution ratios of 1:1 and 3:1, respectively. Powder x-ray diffraction (XRD) measurements identified the precipitates as FeO(OH) and (FeCr)<sub>2</sub>O<sub>3</sub> (data not shown). Cr-XANES spectra of these precipitates showed no evidence of a

Cr(VI) pre-edge feature at 5993 eV, indicating that all of the associated Cr was present as Cr(III) (Fig. 2).

The extent of Cr(VI) reduction increased with increasing concentration of dissolved Fe(II) (Fig. 1), but even when the Fe(II) was 3 times > the concentration of dissolved Cr(VI), only partial reduction was observed. The presence of  $\text{NO}_3^-$  and  $\text{CO}_3^{2-}$  had no effect on Cr(VI) reduction or precipitate formation, nor were reactions at 25°C discernibly different than at 50°C (data not shown). Clearly, rapid reduction Cr(VI) by dissolved Fe(II) is possible in hyperalkaline solutions. Thus, reduction of Cr(VI) to Cr(III) by Fe(II) could have occurred in beneath the HLW tanks if sufficient Fe(II) was present in solution.

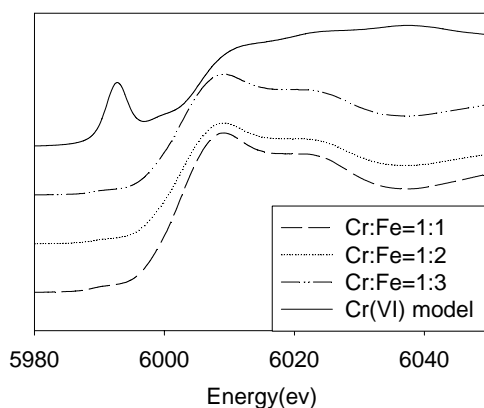


Figure 2. Cr-XANES spectra of Cr(VI) model and the Cr-Fe precipitates from the homogenous reduction experiment.

## B. Cr(VI) reduction in heterogeneous systems.

The reduction of Cr(VI) by Fe(II)-containing minerals is well documented (Citations). While these systems are intrinsically heterogeneous, Cr(VI) reduction can still occur by either a heterogeneous or a homogeneous pathway. In the former, Cr(VI) reduction occurs after the chromate anion reacts with an Fe(II) containing particle surface. The Fe(II) may either be structural or adsorbed to surface functional groups. Homogeneous reduction of Cr(VI) by Fe(II) can occur in heterogeneous systems subsequent to the release of Fe(II) to solution from particle surfaces or crystal lattices. Whereas, these reactions have been observed in acidic to circumneutral pH, information in hyperalkaline solutions is lacking. We have explored this area by conducting batch studies of Cr(VI) reduction by Fe(II)-containing solids at pH values > 13.

### *Materials*

The materials chosen for this research included a specimen North Carolina, biotite obtained from the mineral collection of the OSU School of Natural Resources, a synthetic magnetite prepared after Schwertmann and Cornell [4], whole, uncontaminated sediment from the Hanford formation, (obtained from the submarine pit at Hanford, WA), and various mineral isolates separated from the Hanford sediments. The total chemical composition of the specimen biotite is given in Table 1.

The percent Fe as Fe(III) is not known and is being measured. The macroscopic biotite was ground in a corundum ball-mill, passed through a 50 $\mu$ m sieve and then washed with ethanol and air dried prior to use. A magnetic fraction was separated from the Hanford sediment to obtain a sample of natural magnetite. This was further purified through the use of a Na-polytungstate density separation. Experiments on biotite, synthetic magnetite and the magnetic fraction of the Hanford sediments were conducted at a solid to solution ratio of 1:100.

**Table 1: characterization of biotite**

Major element	Weight %	Minor elements	Weight %
SiO <sub>2</sub>	37.2	CaO	0.2
Al <sub>2</sub> O <sub>3</sub>	10.9	Na <sub>2</sub> O	0.2
Fe <sub>2</sub> O <sub>3</sub>	16.4	MnO	0.3
MgO	16.8	TiO <sub>2</sub>	2.1
K <sub>2</sub> O	7.2	Surface area (m <sup>2</sup> g <sup>-1</sup> )	7.4

Reactions with whole Hanford sediment were studied at a solid to solution ratio of 1:10. All samples were prepared in Argon-filled glove box, 25 °C treatment were kept in the glove box and 50 °C treatment moved to 50 °C incubator for aging.

Scanning Electron Microscopy (SEM), X-Ray Diffraction (XRD) and X-Ray Absorption Near Edge Structure (XANES) were used to study the solid phase of these systems. EXAFS analysis yields information about the coordination number, bond distances, type of neighbors, and the local disorder. XANES provides information about the oxidation states *in situ*. Inductively coupled Plasma Spectroscopy (ICP), Graphite furnace AA was used to analyze total Cr, Si, Al, Fe and K in the solution, and UV-visible Spectroscopy was used to analyze Cr(VI) and Fe(II) in the solution.

### Results

Reaction of biotite with NaOH, in the absence of dissolved Cr, resulted in rapid dissolution and release of Fe, Si, Al and K to solution Fig. 3. Colorimetric analyses indicated that all dissolved Fe was Fe(II). Dissolution rates increased with increased NaOH concentration. Fe, K and Al all exhibited rapid release with maximum concentration occurring < 100 hr. Si release did not exhibit and initial maximum value. For the greatest initial concentration of NaOH, Si continued to be released to solution throughout the experiment. SEM micrographs of the NaOH weathered biotite showed rounded edges (from dissolution) and the formation of needle-shaped reaction products Fig 4., but reaction products could not be detected with powder XRD.

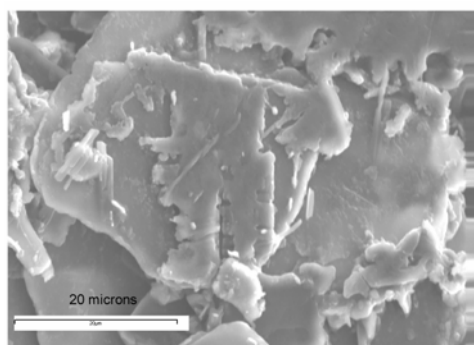


Figure 4. SEM micrograph of biotite reacted for 1500 h with 2 mol L<sup>-1</sup> NaOH.



Figure 3. Dissolution of biotite in NaOH

Brown precipitates were observed at time intervals in excess of 200 h suggesting the precipitation of Fe solids, when Cr(VI) was present in the samples. No precipitates were observed in the absence of Cr(VI). Millimolar levels of chromate had no effect on the dissolution of biotite in NaOH (data not shown). However, reaction of Cr(VI) with biotite in the presence of 1 mol L<sup>-1</sup> NaOH at 50°C did result in sorption of Cr (Fig. 5). Samples containing 10 and 100 μmol L<sup>-1</sup> did not reach apparent equilibrium until reaction times > 100 d and at an initial CrO<sub>4</sub><sup>2-</sup> concentration of 1 mmol L<sup>-1</sup> continued Cr sorption was observed for times > 200 d. It is not reasonable to assume that the CrO<sub>4</sub><sup>2-</sup> anion will *adsorb* to biotite surfaces in 1 mol L<sup>-1</sup> NaOH. Rather it is likely that the Fe(II) released by base-induced dissolution of biotite caused the reduction of Cr(VI) to Cr(III) and subsequent precipitation of a Cr(III) phase or a mixed Fe-Cr (hydr)oxide. Indeed Cr K-edge XANES measurements showed that only Cr(III) was present (data not shown). Increased NaOH concentration led to increased rates of dissolution of the biotite (data not shown) and greater Cr sorption (Fig. 6). Using XPS to study biotites reaction with acidic Cr(VI) solutions, Ilton and Veblen [5] found that Cr is strongly sorbed by the edges of mica books relative to the basal plane, and that much of the Cr associated with the basal plane was sorbed by steps and layer edges. However, this Cr could not be detected with SEM nor was it able to elucidate Cr-rich precipitates.

Several experimental studies have shown that oxidation-reduction reactions between aqueous species and structural Fe(II) on or beneath the surface of both silicates and oxides can result in the heterogeneous reduction of Cr(VI). Peterson and coworkers [6] provide evidence for Cr(VI) reduction at magnetite surfaces. Gan et al [7] showed that Cr(VI) directly reacted with an Fe(II)-containing smectite, forming precipitates on the smectite surface. Ilton and Veblen [8] demonstrated that Cr(VI) could be sorbed and reduced to Cr(III) at the biotite edge-fluid interface by structural Fe(II).

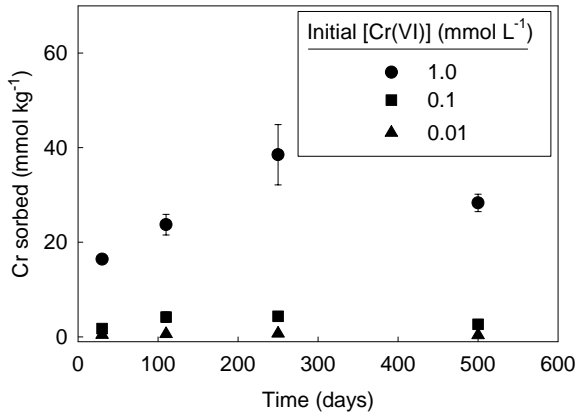


Figure 5. Sorption of Cr by biotite in the presence of 1 mol L<sup>-1</sup> NaOH.

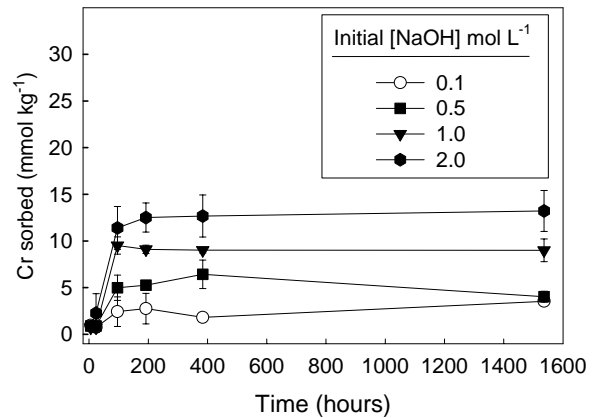


Figure 6. Effect of NaOH concentration on Cr sorption by biotite.

Taylor et al [9] showed that the capacity of artificially reduced clays to reduce Cr(VI) is correlated with the ferrous iron content. The Cr(VI) removal-capacity varied with the clay mineral type in the order smectites > vermiculites ~ illites > kaolinite. Within the same type of clay minerals, reduction of Cr(VI) was correlated to the However, these findings were under acid conditions, nevertheless, Cr(VI) reduction was related to the amount of Fe(II) released during dissolution of the clays. The extent to which Cr(VI) by Fe(II) in the present study is due to *in situ* heterogeneous vs. dissolution followed by homogeneous reduction is not known. However, the increase in Cr(VI) reduction with increased NaOH suggests that dissolution is required before significant Cr(VI) reduction occurs.

The HLW fluids at the Hanford site are high in NO<sub>3</sub><sup>-</sup>, that one might anticipate would inhibit Cr(VI) reduction by Fe(II) by oxidizing the Fe. Interestingly, we observed an increase in the sorption of dissolved Cr(VI) by biotite when 1 mol L<sup>-1</sup> NaNO<sub>3</sub> was present (Fig. 7). Cr K-edge XANES measurements again indicated that all of the Cr associated with the solid phase reaction products was Cr(III) and colorimetric analyses showed the dissolved Cr to consist exclusively of Cr(VI). NaNO<sub>3</sub> also enhanced the release of K from the biotite (Fig. 8). It seems likely that the greater Na<sup>+</sup> concentrations in the NaNO<sub>3</sub> enhanced the weathering of the mica particles through cation exchange displacement of K<sup>+</sup>

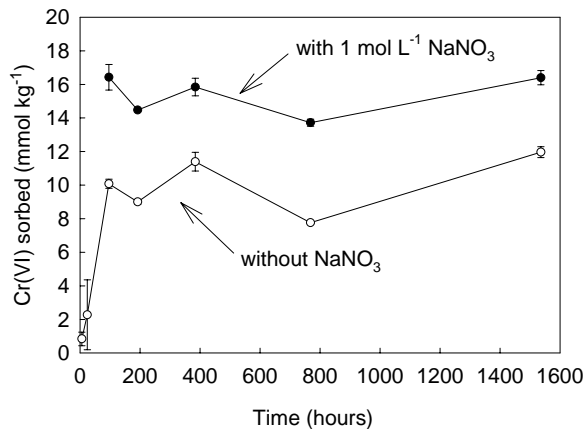


Figure 7. Effect of  $\text{NaNO}_3$  on  $\text{Cr(VI)}$  sorption by biotite in the presence of  $1 \text{ mol L}^{-1} \text{ NaOH}$ .

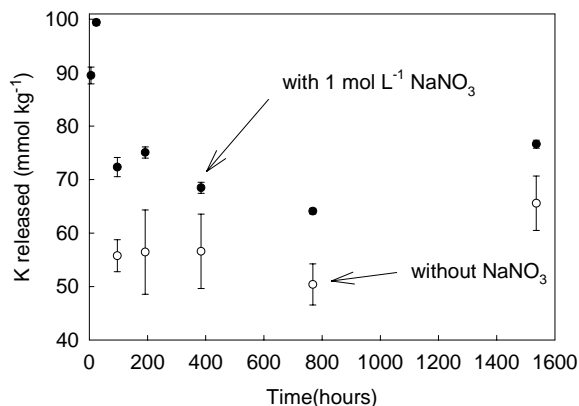


Figure 8. Effect of  $\text{NaNO}_3$  on K release from biotite in the presence of  $1 \text{ mol L}^{-1} \text{ NaOH}$ .

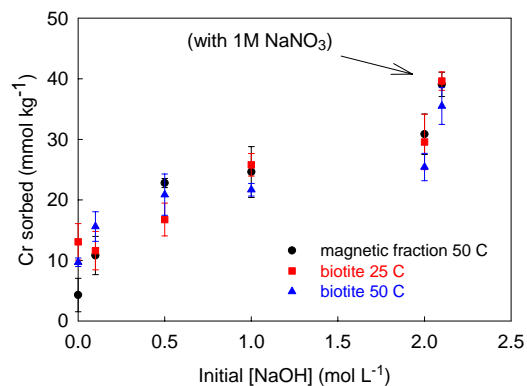


Figure 9. Effect of temperature and  $[\text{NaOH}]$  on  $\text{Cr}$  sorption by the magnetic fraction of the Hanford

exposing more  $\text{Fe(II)}$  to  $\text{Cr(VI)}$ .  $\text{Fe(II)}$  may also have been displaced from cation exchange sites by the greater levels of  $\text{Na}$  ions. The net result was more  $\text{Cr(VI)}$  removal and reduction.

The greater reducing power of solid phase  $\text{Fe(II)}$  relative to aqueous  $\text{Fe(II)}$  is well known. White and Yee [10] demonstrated that ferrous iron in biotite, augite and hornblende was a stronger reducing agent over a broad range of conditions than  $\text{Fe(II)}_{\text{aq}}$ .

We explored the ability of a synthetic magnetite to reduce  $\text{Cr(VI)}$  in the presence of  $1 \text{ mol L}^{-1} \text{ NaOH}$ . We detected minimal removal of  $\text{Cr}$  from solution over the course of 2 weeks and thus little evidence of  $\text{Cr(VI)}$  reduction. These results are not surprising in that little interaction is anticipated between the negatively charge magnetite ( $\text{PZNC} \approx 8$ ) and the  $\text{CrO}_4^{2-}$  ion under the conditions of these experiments. Indeed, Zachara and others [11] have shown that chromate is not adsorbed onto iron oxides at  $\text{pH}$  values  $> 11.5$ . Figure 9 compares the removal of  $\text{Cr(VI)}$  by the specimen biotite described above and by the magnetic fraction of the Hanford sediment. In contrast to the results observed for the synthetic magnetite, this fraction appeared to be roughly equivalent to the synthetic magnetite in its ability to remove  $\text{Cr}$  from solution. Careful examination of this sediment fraction by light microscopy and powder XRD indicated the presence of biotite, and other primary minerals. Based on our studies of synthetic magnetite, we attribute the removal of  $\text{Cr}$  by the magnetic fraction of the Hanford sediment to dissolution of residual biotites (and other  $\text{Fe(II)}$ -containing phyllo-silicates) and subsequent reduction of  $\text{Cr(VI)}$  by  $\text{Fe(II)}$ . As indicated above, we attempted to further purify the magnetically separated

sediment material by a series of Na-polytungstate density separations. Unfortunately we could not completely remove the biotite with this treatment. However, reaction of this magnetic, higher density fraction with Cr(VI) and 1 mol L<sup>-1</sup> NaOH, yielded a reddish brown precipitate that remained suspended in solution after several days of reaction (Fig. 10). The presence of dominantly Cr(III) in this precipitate was confirmed with Cr XANES spectra (Fig 11).

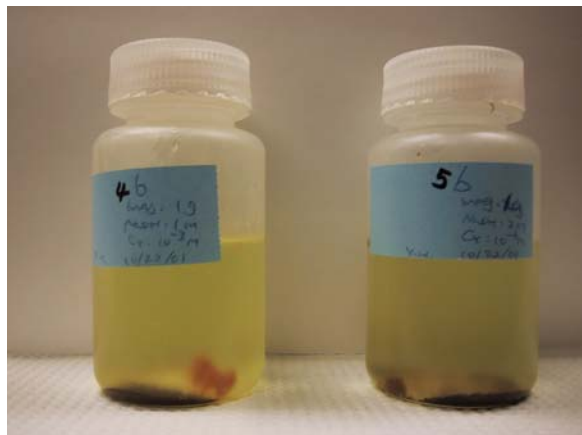


Figure 10. Reddish-brown precipitate from magnetic and density separated sediment fraction from the Hanford sediment. Precipitates formed after reaction with 1 mol L<sup>-1</sup> NaOH and 1 mmol L<sup>-1</sup> Na<sub>2</sub>CrO<sub>4</sub>.

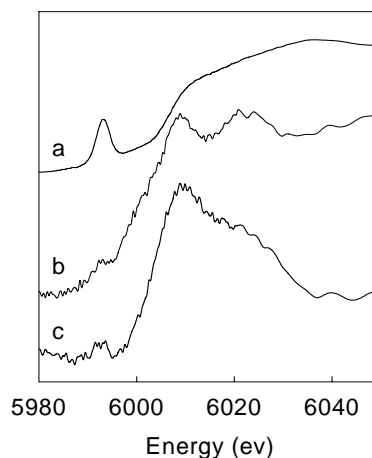


Figure 11. Cr XANES spectra of a) Na<sub>2</sub>CrO<sub>4</sub>, b) the dark magnetic fraction from figure 10 and c) the suspended precipitate from figure 10.

Reaction of the Hanford sediment with varying amounts of NaOH resulted in dissolution and release of Si, Al and K. Interestingly, more Cr was sorbed in the presence of NO<sub>3</sub><sup>-</sup> than in NO<sub>3</sub><sup>-</sup>-free, NaOH solutions (Fig. 12 and Fig.13). This again may be due to Na-induced displacement of Fe(II) from particle surfaces.

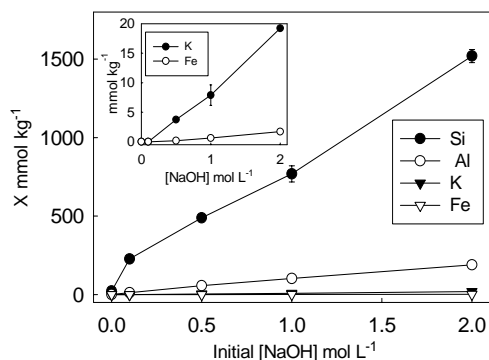


Figure 12. Weathering of Hanford sediment in NaOH.

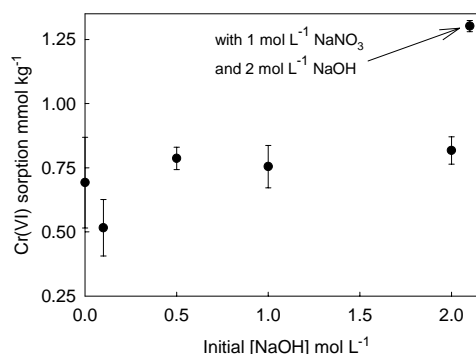


Figure 13. Effect NaOH on Cr sorption by Hanford sediment. Note: last sample was reacted in the presence of 1 mol L<sup>-1</sup> NaNO<sub>3</sub>.

### C. Incorporation of Cr(VI) into Al-precipitates

The HLW fluids from the redox process were typified by high concentrations of dissolved Al ( $> 0.1 \text{ mol L}^{-1}$ ). Upon reaction with a soil matrix, these Al-rich alkaline solutions dropped in pH resulting in the precipitation of Al-(hydr)oxide phases. Al-precipitation also resulted from  $\text{OH}^-$  induced weathering of alumino-silicates present in the soil and sedimentary materials.

Incorporation of  $\text{CrO}_4^{2-}$  into these precipitates is possible. Bartlett and Kimble [12] showed that in the presence of Al in the solution, Cr(VI) was precipitated as the pH was increased above 4-5, it became almost completely insoluble near pH 6 and increased in solubility again above 8. Cr(VI) was probably coprecipitated with the Al. The enhanced solubility of Cr at pH values  $> 8$  in Bartlett and Kimble's study was likely do to dissolution of the Al-phases. However, the HLW fluids were saturated with respect to Al-(hydr)oxides and thus coprecipitation is possible even at extremely high pH values. We evaluated the potential incorporation of  $\text{CrO}_4^{2-}$  into Al-precipitates by aging solutions of  $1 \text{ mol L}^{-1} \text{ Al}(\text{NO}_3)_3$  and from 0.52 to 52 mmol of  $\text{Na}_2\text{CrO}_4 \text{ L}^{-1}$  with  $4 \text{ mol L}^{-1} \text{ NaOH}$ . Within 1 week extensive Al precipitation occurred. Interestingly, the extent of Al precipitation increased with increased initial concentrations of Cr. From 20.6 to 23.1% of the total dissolved Cr was removed in these treatments. XANES spectra showed that the Cr remained as Cr(VI) (data not shown) but only gibbsite was detected by powder XRD. Similar results were observed in samples comprised of hyperalkaline Na-aluminate solutions reacted with amorphous  $\text{SiO}_2$ , in the presence of Cr(VI). Indeed the dissolved Cr(VI) concentrations in these systems reached a constant value after approximately 2 weeks and have remained constant for periods in excess of 1 year. Apparently Cr(VI) incorporation into Al-precipitates may be a mechanism for Cr(VI)-retardation in near-field to the HLW tanks.

### References:

- [1] R. R. Patterson and S. Fendorf, 1997, Reduction of hexavalent chromium by amorphous iron sulfide, *Environmental Science and Technology*, 31, 2039-2044.
- [2] L.E. Eary and D. Rai, 1988, Chromate removal from aqueous wastes by reduction with ferrous iron, *Environmental Science and Technology*, 22, 972-977.
- [3] I. J. Buerge and S. J. Hug, 1999, Influence of mineral surfaces on chromium(VI) reduction by iron(II), *Environmental Science and Technology*, 33, 4285-4291.
- [4] U. Schwertmann and R.M. Cornell, 1991, Magnetite, in *Iron oxides in the laboratory*, VCH, Inc., New York, pp.111-116.
- [5] E. S. Ilton and D. R. Veblen, 1994, Chromium sorption by phlogopite and biotite in acidic solutions at 25 C: insights from X-ray photoelectron spectroscopy and electron microscopy, *Goechimica et Cosmochimica Acta*, Vol.58, No.13, pp.2777-2788.
- [6] M. L. Peterson et al, Direct XAFS evidence for heterogeneous redox reaction at the aqueous chromium/magnetite interface, *Colloids and Surfaces A*, 1996, Vol.107, 77-88.

- [7] H.G. Gan et al, Morphology of lead(II) and chromium(III) reactions products on phyllosilicate surface as determined by atomic force microscopy, *Clays and Clay minerals*, 1996, Vol.44, 734-743.
- [8] E. S. Ilton et al, 1997, The catalytic effect of sodium and lithium ions on coupled sorption reduction of chromate at the biotite edge-fluid interface, *Geochimica et Cosmochimica Acta*, Vol.61, No.17, pp.3543-3563.
- [9] R. W. Taylor et al, 2000, Chromate removal by dithionite-reduced clays: evidence from direct X-ray absorption near edge spectroscopy (XANES) of chromate reduction at clay surfaces, *Clays and Clay Minerals*, Vol.48, No.6, 648-654.
- [10] A. F. White et al, Surface oxidation-reduction kinetics associated with experimental basalt-water reaction at 25C, 1985, *Chemical geology*, V49, 73-86.
- [11] J. M. Zachara, et al, 1987, Chromate adsorption on amorphous iron oxyhydroxide in the presence of major groundwater ions, *Environmental Science and Technology*, 21(6), 589-594.
- [12] R.J. Baetlett and J.M. Kimble, 1976, Behavior of chromium in soils: I. Trivalent forms, *Journal of Environmental Quality*, Vol. 5, No.4, 379-386.

## PRECIPITATION AND ADSORPTION OF URANIUM IN HIGHLY ALKALINE SOLUTIONS: POSSIBLE CHEMICAL REACTIONS OCCURRING IN THE HANFORD VADOSE ZONE BENEATH THE TANK FARM.

**Abstract-**This study has investigated precipitation and adsorption of U(VI) in highly alkaline solutions related to Hanford Tank fluid conditions using EXAFS spectroscopy. Under high concentration of NaOH (1.0~4.0M, pH>13), uranyl ion ( $\text{UO}_2^{2+}$ ) yielded yellow precipitate identified as  $\text{Na}_2\text{U}_2\text{O}_7$  (clarkeite). The very low U concentration in the liquid phase indicates that > 99% of total  $\text{UO}_2^{2+}$  precipitated in the form of  $\text{Na}_2\text{U}_2\text{O}_7$ . This precipitation process was not affected neither by high concentration of carbonate ions (< 1.5M as  $\text{Na}_2\text{CO}_3$ ) nor by presence of  $\text{CaCO}_3$ . In the presence of  $\text{Al}^{3+}$  at  $10^{-4}\text{M} < \text{UO}_2^{2+}$ ,  $\text{Na}_2\text{U}_2\text{O}_7$  coprecipitated with aluminum hydroxide,  $\text{Al}(\text{OH})_3$  (gibbsite, bayerite, and amorphous). However, when the  $\text{UO}_2^{2+}$  concentration was approximately  $10^{-5}\text{M}$ , adsorption on the solid surface exceeded the precipitation. The fits to EXAFS spectra indicate that  $\text{UO}_2^{2+}$  with hydroxide ligands was adsorbed on the surface of  $\text{Al}(\text{OH})_3$  in bidentate form. Similar results were obtained in experiments using Hanford sediments. 1.0~2.0M  $\text{SiO}_2$  prevented  $\text{Na}_2\text{U}_2\text{O}_7$  formation and kept  $\text{UO}_2^{2+}$  dissolved in a 1.0M NaOH solution.

### INTRODUCTION

Hanford played an important role in the nation's defense for more than 50 year as a Pu production facility. At the Hanford site, waste fluids resulting from the extraction processes were stored in 177 underground tanks during the period of 1944 to 1990, in areas known as "Tank Farm". Many of the tanks are known to have leaked, allowing from large amount of waste fluids to migrate into the underlying vadose zone.

Recently, the Tank Waste Remediation System (TWRS) project has sampled the tank solids and fluids. The aqueous phase data is accessible through Tank Waste Information Network System (TWINS2). The chemical composition of the tank fluids varies because of the many different extraction processes practiced at the Hanford site during the time. Many of these fluids were highly alkaline (pH >13), and contained large concentration of Na and Al. Many types of anions such as nitrate, nitrite, chloride, sulfate, and phosphate were observed in the most of the tanks. Reaction of the highly alkaline tank fluids including a various of chemical species with the underlying soil and sedimentary matrix should cause complex precipitation and dissolution resulting in dramatic changes in the fate and transport of the contaminants associated with the tank fluids.

The primary purpose of this study is to simulate possible chemical reactions on uranium at the Hanford Site. The specific objectives are to investigate; 1) precipitation processes uranium and other elements in the highly alkaline solutions, 2) the interaction of U to the solids formed from reaction of the alkaline aluminate solution with soils and sediments in the Hanford site, and 3) effect of carbonate and silicate on the U mobility.

## EXPERIMENTAL

### Sample Preparation

Experimental design was based on the chemical composition data for the SX tanks which have high total uranium concentration. A primary stock solution of U(VI) was prepared from uranyl nitrate hexahydrate,  $\text{UO}_2(\text{NO}_3)_2 \cdot 6\text{H}_2\text{O}$ . 2.8 mM  $\text{UO}_2(\text{NO}_3)_2$  solution was added into 1.0~4.0M NaOH, and stored in the incubator at 50°C. The temperature is the average value of the elevated temperatures observed beneath the tanks. In order to study effects of other species on U activities,  $\text{Al}(\text{NO}_3)_3$ ,  $\text{Na}_2\text{CO}_3$ ,  $\text{Al}(\text{OH})_3$ ,  $\text{CaCO}_3$ ,  $\text{SiO}_2$ , and Hanford sediments were individually added into the NaOH solution containing  $\text{UO}_2^{2+}$ . All experiments were conducted in an Ar(g)-filled glove box except samples with carbonate compounds.

### Elemental Analysis

Measurement of the solution pH was conducted under Ar gas substituted globe box with a Sentron Intelli Standard FET electrode and Denver Instrument Company Basic pH meter. U, Al, Na, and Si concentrations were measured by ICP-MS (ELAN Sciex 6000, Perkin-Elmer Co., Norwalk, CT) and ICP-OES (Optima 3000, Perkin-Elmer Co., Norwalk, CT) spectroscopy. XRD analysis was performed with a Philips X-ray diffractometer using Cu K $\alpha$  radiation at 35 kV and 20 mA. The XRD patterns were obtained using a step scanning technique with a fixed time of 4 seconds per  $0.05^\circ 2\theta$  from  $10^\circ$  to  $80^\circ 2\theta$ .

### XAFS Data Collections and Analysis

Uranium L<sub>III</sub>-edge X-ray adsorption spectra for all samples were collected at Stanford Synchrotron Radiation Laboratory (SSRL) on beam lines 4-3 and 11-2 using a Si (220) double crystal monochromator. Solid samples were held in 2mm thick Teflon plates and covered by Kapton tape. Liquid samples were placed to 2mL polypropylene tubes and held on the holder with Kapton tape. Fluorescence spectra were collected by 13-element Ge (at BL 4-3) and 30-element Ge (at BL 11-2) array detectors interfaced to a multichannel analyzer using Sr filter to eliminate scattered radiation. Transmission spectra were collected for high concentration samples.

XAFS analysis was performed using the EXAFSPAK software (George and Pickering, 2000) and IFEFFIT (Newville, 2001). The averaged raw absorption spectra were background subtracted, spline-fit, and Fourier-transformed. Backscattering phase and amplitude functions for fitting of spectra were obtained from theoretical calculation (FEFF8) based on crystal structures of clarkeite,  $\text{Na}_2\text{U}_2\text{O}_7$  and soddyite,  $(\text{UO}_2)_2\text{SiO}_4$ .

## RESULTS AND DISCUSSION

### Uranium precipitation

Mixing 2.8mM  $\text{UO}_2^{2+}$  and 1.0~4.0M NaOH solution immediately yielded a yellow precipitate identified as sodium diuranate,  $\text{Na}_2\text{U}_2\text{O}_7$  (clarkeite) by X-ray powder

diffraction (Fig.1). U concentration in the liquid phase was very low as  $1 \mu\text{M}$ , indicating that  $> 99.5\%$  of total U was precipitated in the form of  $\text{Na}_2\text{U}_2\text{O}_7$ . The original  $\text{UO}_2(\text{NO}_3)_2$  stock solution had a pH of 4. As the NaOH concentration increased, pH increased and the U concentration decreased (Fig.2). Na concentration  $> 10^{-2}\text{M}$  and pH values  $> 11$  resulted in precipitation of clarkeite.  $\text{Na}_2\text{U}_2\text{O}_7$  dissolution was observed only when the solution pH was reduced to 3 to 4. Considering the tank fluid conditions present in the TWINS database, U in the SX tanks is expected to be immobilized as  $\text{Na}_2\text{U}_2\text{O}_7$ .

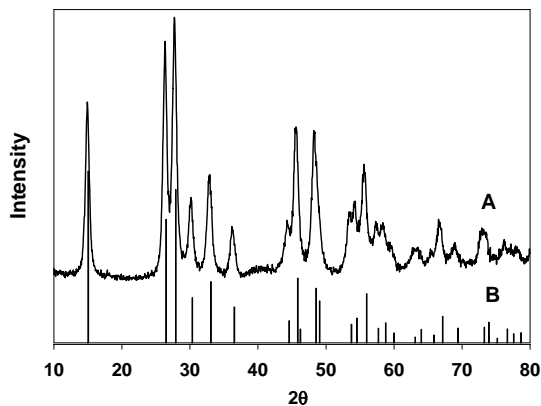


**Figure 1.** X-ray powder diffraction diagram for the precipitate obtained from  $\text{UO}_2^{2+}$  and 4M NaOH solution (A), compared with the diffraction pattern calculated with crystal information of clarkeite,  $\text{Na}_2\text{U}_2\text{O}_7$  (B) (Finch and Ewing, 1997)

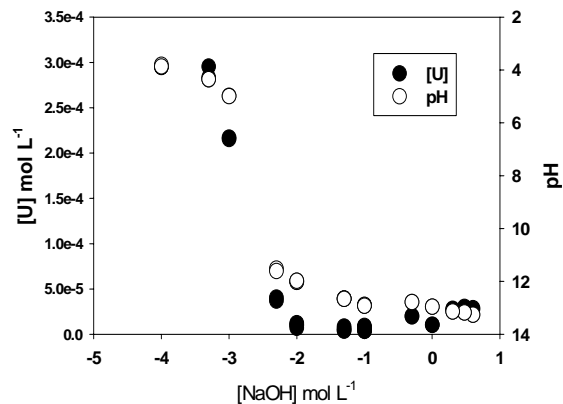


**Figure 2.** Correlation of uranium concentration with pH changes corresponding to NaOH concentration. At pH more than 11 and high Na conc. ( $> 10^{-2}\text{M}$ ), U was precipitated as clarkeite,  $\text{Na}_2\text{U}_2\text{O}_7$ .

### Effect of $\text{CO}_3^{2-}$ on uranium dissolution/precipitation

Generally, in the presence of  $\text{CO}_3^{2-}$  in alkaline solutions,  $\text{UO}_2^{2+}$  forms stable complexes like uranyl carbonate, hydroxyl, and carbonato-hydroxo complexes (Waite et al., 1994; Murphy et al., 1999). Also, it is reported that 0.1M  $\text{CO}_3^{2-}$  resulted in  $\text{Na}_2\text{U}_2\text{O}_7$  dissolution in highly basic solutions (Yamamura et al., 1998). In the present study, 0.28 mM  $\text{UO}_2(\text{NO}_3)_2$  solution was added into different concentrations of  $\text{CO}_3^{2-}$  (0.05~1.50M as  $\text{Na}_2\text{CO}_3$ ) in 1M NaOH solution to study the effect of  $\text{CO}_3^{2-}$  on uranium dissolution.  $\text{NaNO}_3$

was also added to keep total Na concentration constant. All samples were stored at  $50^\circ\text{C}$ . There is very little change in dissolved U concentration across the composition space (Fig.3), and clarkeite formation was observed in the all samples. This suggests that  $\text{CO}_3^{2-}$  did not dramatically affect U solubility or clarkeite formation under the conditions of these measurements. Indeed the solution composition was invariant for the 6-month duration of this experiment.

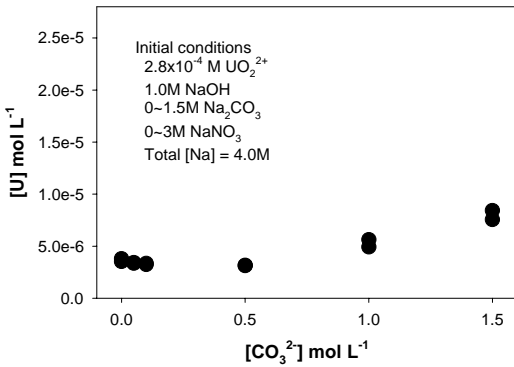


**Figure 3.** U concentration was very low and unchanged in different concentration of  $\text{CO}_3^{2-}$  (<1.5M) with  $\text{NaNO}_3$  and 1M NaOH. Total Na concentration was constant as 4.0M.  $\text{Na}_2\text{U}_2\text{O}_7$  formation was observed in each solution.

Fig.4 shows  $\text{Na}_2\text{U}_2\text{O}_7$  solubility calculated with the chemical speciation program, Phreeqc using the LLNL database. This calculation was without  $\text{CO}_2$ .  $\text{Na}_2\text{U}_2\text{O}_7$  dissolution equilibrium is controlled by the Na concentration and pH. As pH decreases and Na concentration decreases, U concentration increases. However, the U concentration is in the micromolar range, indicating that the solubility of clarkeite is low under these conditions. Figure.5 show the same calculation with  $P_{\text{CO}_2} = 10^{-3.5}$  (A) and  $P_{\text{CO}_2} = 10^{-2.5}$  (B). Under partial pressure  $10^{-3.5}$  (atmospheric conditions) the U concentration is about 10 times > without  $\text{CO}_2$ . When the partial pressure is  $10^{-2.5}$ , the U concentration jumped up to 100 times > than in the absence of  $\text{CO}_2$ . Clearly the disposition of U near-field to a tank leak will be a function of the sediment pH, the total Na concentration and the local  $P_{\text{CO}_2}$ .

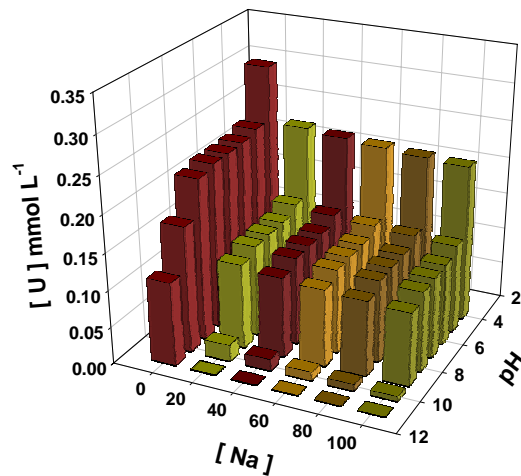


**Figure 4.**  $\text{Na}_2\text{U}_2\text{O}_7$  solubility calculation with chemical speciation program without  $\text{CO}_2$  factor

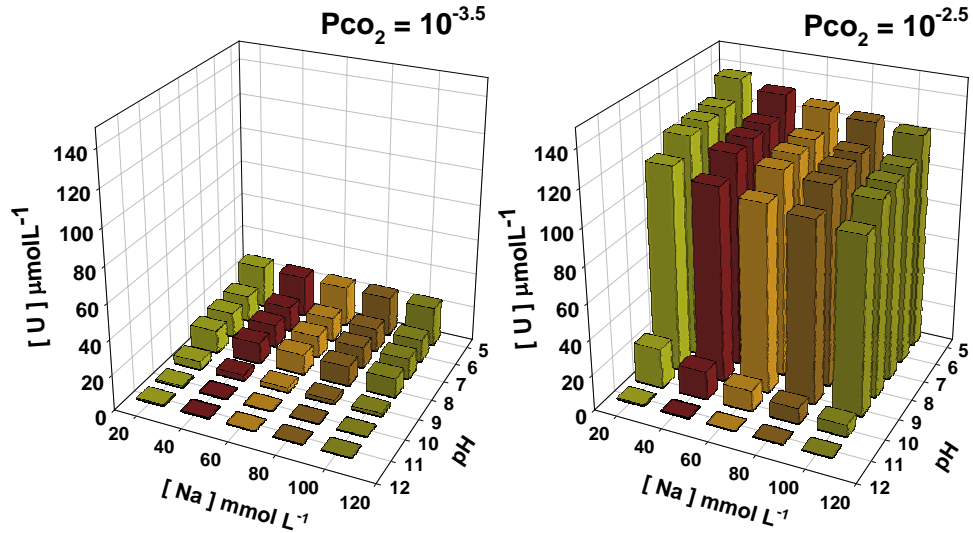


**Figure 5.**  $\text{Na}_2\text{U}_2\text{O}_7$  solubility calculation with chemical speciation program with considering presence of  $\text{CO}_2$ ,  $P_{\text{CO}_2}=10^{-3.5}$  (A),  $P_{\text{CO}_2}=10^{-2.5}$  (B)

### U coprecipitation with $\text{Al}(\text{OH})_3$ and U adsorption on $\text{Al}(\text{OH})_3$

When aluminosilicate minerals are exposed to very high pH solutions, Al is released by dissolution. This dissolved aluminate ion,  $\text{Al}(\text{OH})_4^-$ , could reform other types of solids; thus, we explored the effects of dissolved Al on U chemistry.

When 1.0 ~ 4.0M NaOH solution was added to a 1 M  $\text{Al}(\text{NO}_3)_3$ , in the absence of  $\text{CO}_2$ , a OH:Al ratio of 1:3.0 - 4.3 resulted in the formation of  $\text{Al}(\text{OH})_3$  as both gibbsite and bayerite (Fig.6). The presence of  $\text{CO}_3^{2-}$  affected gibbsite/bayerite formation. Bayerite formation was most pronounced when  $\text{CO}_3^{2-}$  was  $10^{-3}\text{M}$  in OH:Al=3.3 (Fig.7) When the OH:Al ratio was higher than 4.5, Al was completely dissolved in the form of  $\text{Al}(\text{OH})_4^-$ . Amorphous aluminum (hydr)oxide formed when the ratio was lower than 3.0.

NaOH. Gibbsite and bayerite formation depends on OH:Al ratio. Arrows with "B" indicate major peaks of bayerite.

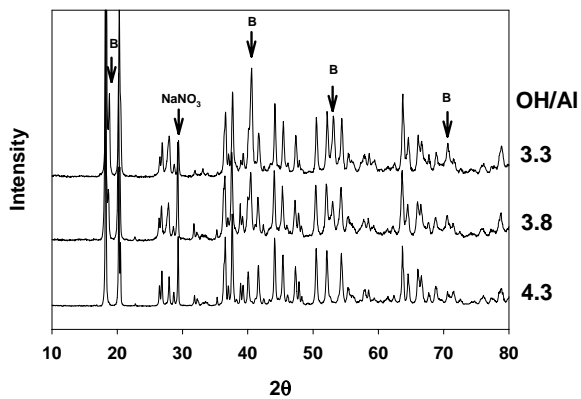


**Figure 6.** X-ray diffraction patterns of  $\text{Al}(\text{OH})_3$  produced from  $\text{Al}(\text{NO}_3)_3$  and

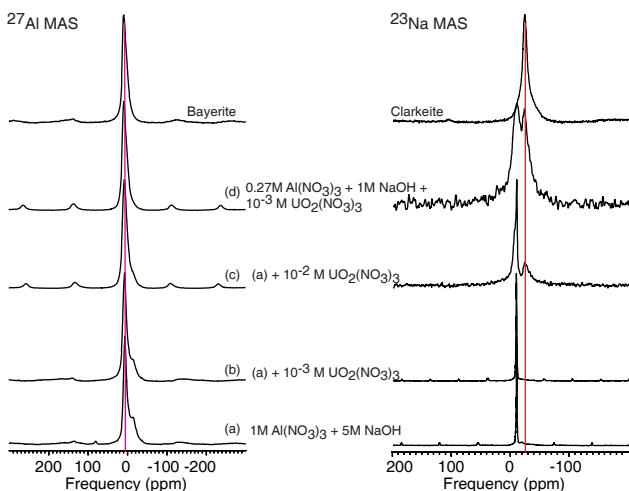


**Figure 7.** X-ray diffraction patterns of  $\text{Al}(\text{OH})_3$  produced from  $\text{Al}(\text{NO}_3)_3$  and  $\text{NaOH}$  with  $\text{CO}_3^{2-}$ . Effect of  $\text{CO}_3^{2-}$  on gibbsite and bayerite formation in  $\text{NaOH}$  solution

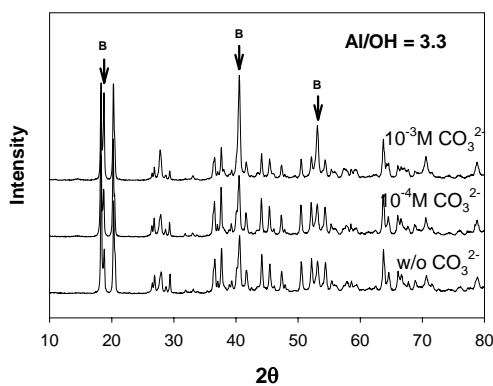


**Figure 8.**  $^{27}\text{Al}$  NMR and  $^{23}\text{Na}$  NMR spectra for solids obtained from  $\text{Al}(\text{NO}_3)_3$ ,  $\text{NaOH}$ , and  $\text{UO}_2(\text{NO}_3)_2$  solution, compared with those for bayerite and clarkeite, respectively.

Multinuclear ( $^{27}\text{Al}$  and  $^{23}\text{Na}$ ) techniques such as magic-angle spinning (MAS) and multiple quantum magic-angle spinning (MQ-MAS) were used to determine solid phases produced from  $\text{Al}(\text{NO}_3)_3$  and  $\text{NaOH}$  with and without  $\text{UO}_2(\text{NO}_3)_3$ . The solid was characterized by two Al environments in the  $^{27}\text{Al}$  spectrum and is identified as gibbsite (Fig. 8a). In the presence of added dopants (e.g.,  $10^{-3}$  M  $\text{UO}_2(\text{NO}_3)_3$ ), or under lower  $\text{NaOH}$  concentration, bayerite co-precipitated (Fig.8b). Commercial bayerite shows a single resonance attributed to one crystallographic site. However, due to the narrow range of chemical shift for octahedral aluminum and the presence of significant amount of disorder, overlapping of resonances occur. Thus, identification of different phases or mixtures there of based on observed chemical shift is difficult. Measurement of the spin-lattice relaxation rate constant ( $T_1$ ) is an useful tool in such cases. The measured  $T_1$  of gibbsite and bayerite are widely different (240 ms and 360 ms, respectively), and the  $T_1$  for other samples (containing mixtures), fall in between. Isotropic spectra were also obtained by multiple quantum MAS spectroscopy and NMR parameters were extracted.

$^{23}\text{Na}$  MAS measurements indicated, in addition to  $\text{NaNO}_3$ , the formation of  $\text{Na}_2\text{U}_2\text{O}_7$  in certain samples where uranium nitrate concentration was high.

To explore the interactions of U(VI) with Al-precipitates, a wide range of  $\text{UO}_2^{2+}$  solution (0.028~2.8 mM) was added to 1M NaOH solutions with 0.27M  $\text{Al}(\text{NO}_3)_3$ . The samples were kept at 50°C. The dissolved U concentration was low (1  $\mu\text{M}$ ), indicating that most of total U was in the solid phase, but no clarkeite could be detected by powder XRD. Fig. 9 shows U EXAFS and the corresponding Fourier Transforms (FT) for synthesized clarkeite (A) and solids obtained from  $\text{UO}_2(\text{NO}_3)_2$  and  $\text{Al}(\text{NO}_3)_3$ , in 1M NaOH (pH>13). The  $\text{UO}_2^{2+}$  concentration was 2.8mM (B), 0.28mM (C), and 0.028mM (D). Similar patterns of EXAFS and peak positions in RDFs in B and C indicate bond distances and coordination numbers consistent with clarkeite or a clarkeite-like phase. The peaks around 3.9Å are attributed to the U-U scattering path in  $\text{Na}_2\text{U}_2\text{O}_7$ . As the  $\text{UO}_2^{2+}$  concentration decreased, the relative height of the U- $\text{O}_{\text{eq}}$  peaks got larger. The lowest  $\text{UO}_2^{2+}$  sample's spectra (D) did not show the U-U path (3.9Å), and a new peak appeared near 3.3Å. This peak is attributed to a U-Al scattering path. The fits to EXAFS spectra (Fig.10 and Table 1) indicate that  $\text{UO}_2^{2+}$  with hydroxide ligands was adsorbed on the surface of  $\text{Al}(\text{OH})_3$  in a bidentate form by sharing two of five equatorial oxygens with octahedral aluminum in  $\text{Al}(\text{OH})_3$  (Fig.11). In conclusion, with higher  $\text{UO}_2^{2+}$  concentration ( $> 10^{-4}\text{M}$ ),  $\text{Na}_2\text{U}_2\text{O}_7$  coprecipitated with  $\text{Al}(\text{OH})_3$ . When the  $\text{UO}_2^{2+}$  concentration was low as  $10^{-5}\text{M}$ , however, adsorption on the solid surface exceeded the precipitation.

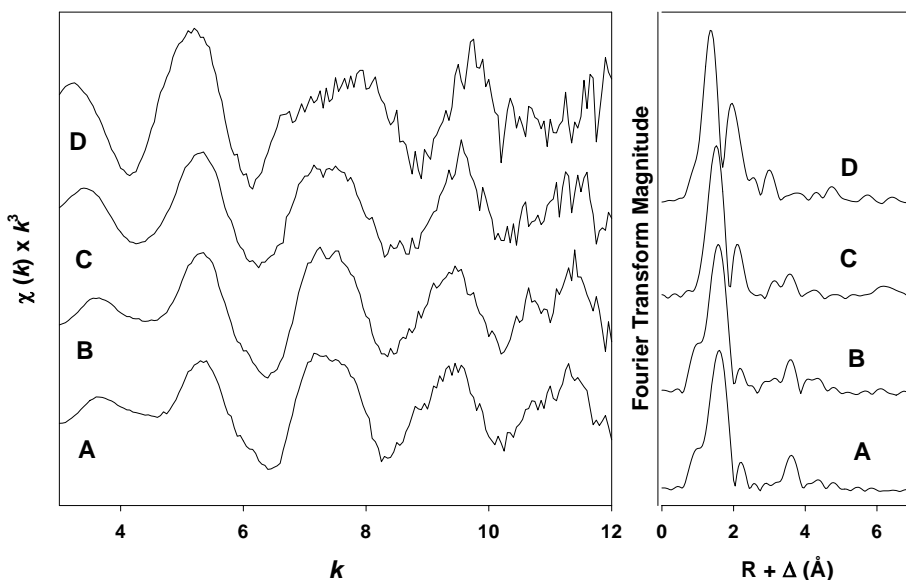


**Figure 9.** Uranium EXAFS spectra and the corresponding Fourier Transforms for  $\text{Al}(\text{OH})_3$  with 2.8mM  $\text{UO}_2^{2+}$  (B), 0.28mM  $\text{UO}_2^{2+}$  (C), and 0.028mM  $\text{UO}_2^{2+}$  (D), compared with those for  $\text{Na}_2\text{U}_2\text{O}_7$  (A).

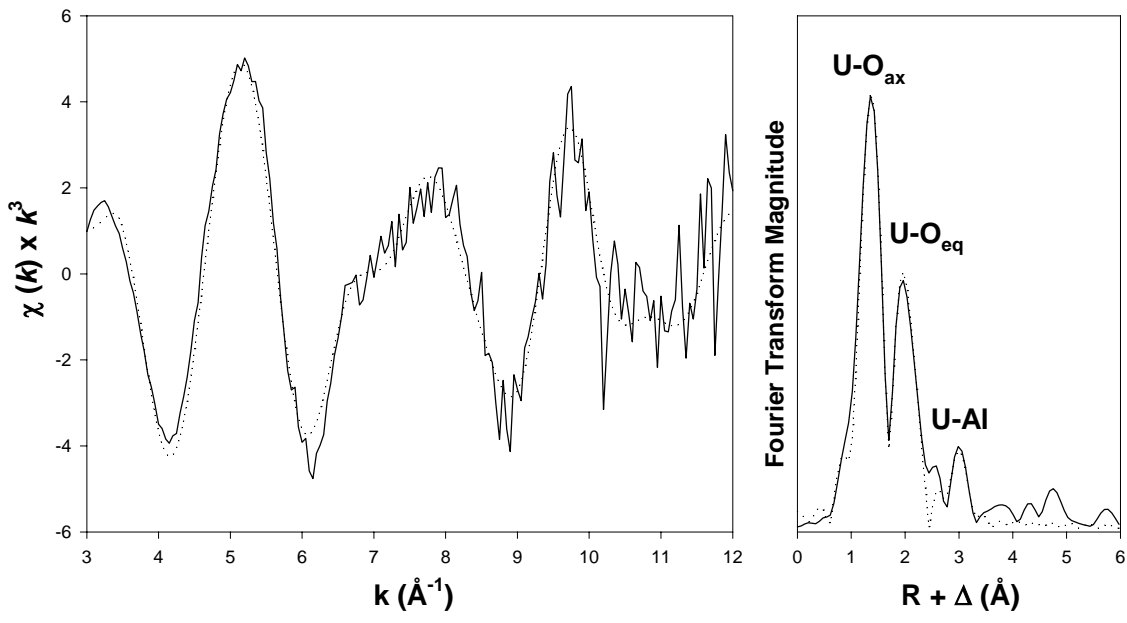


**Figure 10.** Uranium EXAFS and RDFs for 0.028mM  $\text{UO}_2^{2+}$  on  $\text{Al}(\text{OH})_3$ . Solid lines are experimental data and dashed lines represent the fits.

**Table 1.** EXAFS results for 0.028mM  $\text{UO}_2^{2+}$  with  $\text{Al}(\text{OH})_3$  produce from 0.27M  $\text{Al}(\text{NO}_3)_3$  and 1.0M NaOH.

sample	scattering path	N	R (Å)	$\sigma^2$	$E_0$
0.028mM $\text{UO}_2(\text{NO}_3)_2$ with $\text{Al}(\text{OH})_3$	U- $\text{O}_{\text{ax}}$	2.14	1.79	0.0026	14.3
	U- $\text{O}_{\text{eq1}}$	1.99	2.35	0.0060	14.3
	U- $\text{O}_{\text{eq2}}$	2.82	2.49	0.0023	14.3
	U-Al	1.11	3.32	0.0025	14.3

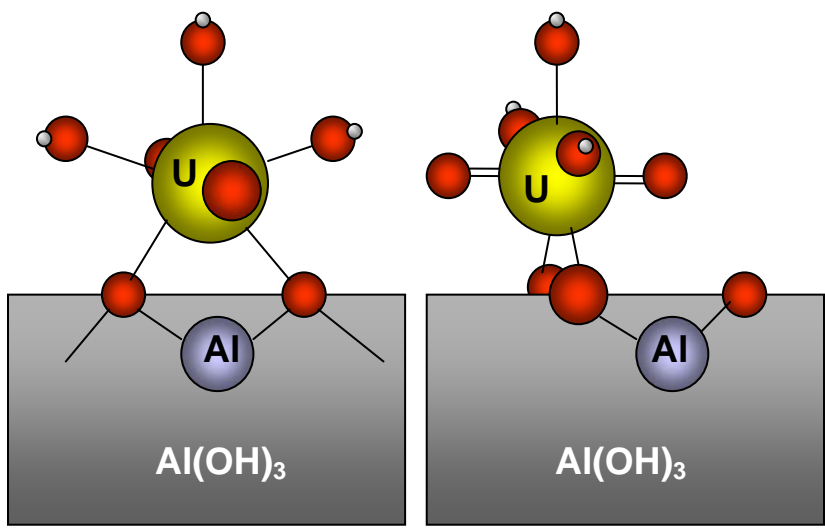


**Figure 11.** Model structure for uranyl hydroxide complex adsorbed on  $\text{Al}(\text{OH})_3$  surfaces, showing two of five equatorial oxygen atoms shared with the aluminum octahedron.

### U precipitation and adsorption on Hanford sediments

Results similar to those observed for model solutions were obtained in experiments using Hanford sediments (Fig.12). Different concentrations of  $\text{UO}_2^{2+}$  (0.28mM~2.80mM) were added to 1M NaOH containing 1% (by weight) uncontaminated Hanford sediments. THE EXAFS patterns and peak positions in RDFs for solid obtained from 2.8mM  $\text{UO}_2^{2+}$ , 1M NaOH, and Hanford sediments (B) are very similar to those for clarkeite,  $\text{Na}_2\text{U}_2\text{O}_7$  (A) indicating clarkeite formation in these samples. When the  $\text{UO}_2^{2+}$  concentration was low (0.28mM), the U-EXAFS and corresponding FTs were comparable to those for sample D in Fig. 9, indicating sorption of a uranyl hydroxide complex.

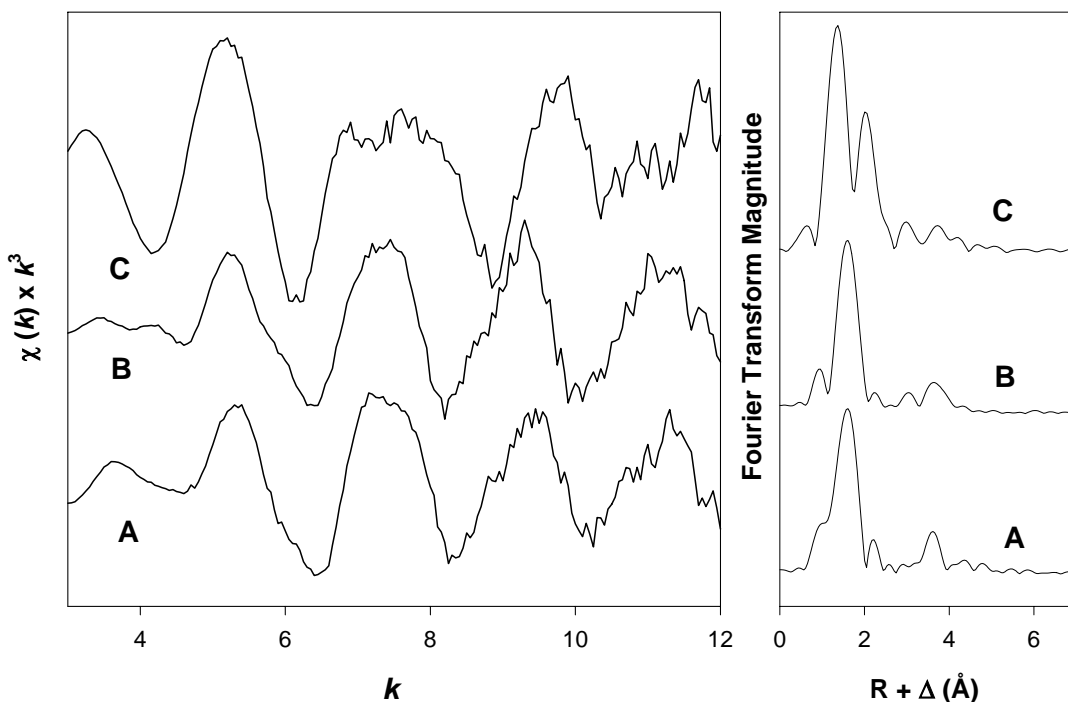


**Figure 12.** Uranium EXAFS spectra and the corresponding Fourier Transforms for Hanford sediments samples with 2.8mM  $\text{UO}_2^{2+}$  (B) and 0.28mM  $\text{UO}_2^{2+}$  (C), compared with those for  $\text{Na}_2\text{U}_2\text{O}_7$  (A).

### Effect of $\text{SiO}_2$ on U dissolution and precipitation

The solid phases produced from  $\text{UO}_2(\text{NO}_3)_2$ ,  $\text{Al}(\text{NO}_3)_3$ , NaOH, and  $\text{SiO}_2$  were analyzed by multinuclear NMR ( $^{27}\text{Al}$ ,  $^{23}\text{Na}$ , and  $^{29}\text{Si}$ ) using MAS and MQ-MAS techniques. In the solids precipitated from gels containing  $\text{SiO}_2$ , in addition to the presence of octahedral Al sites such as were observed in gibbsite and bayerite (Fig. 13a),  $^{27}\text{Al}$  measurements indicated the presence of tetrahedral Al species including zeolitic

aluminum (Fig. 13b, 13c, and 13d). These tetrahedral sites are different from those present in gamma alumina.  $^{29}\text{Si}$  MAS NMR measurements (not shown) corroborated the presence of Si-O-Al linkages. However, in the presence of added  $\text{SiO}_2$ , clarkeite formation was restricted.

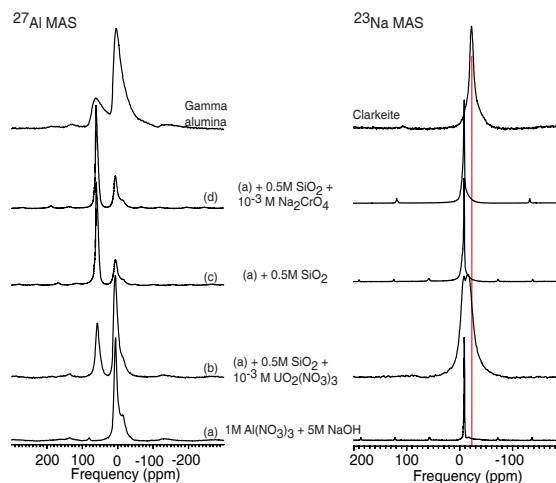


**Figure 13.**  $^{27}\text{Al}$  NMR and  $^{23}\text{Na}$  NMR spectra for solids obtained from  $\text{Al}(\text{NO}_3)_3$ ,  $\text{NaOH}$ ,  $\text{UO}_2(\text{NO}_3)_2$  solution containing  $\text{SiO}_2$ , compared with those for gamma alumina and clarkeite.

To explore the effects of dissolved Si on clarkeite formation,  $0.28\text{mM UO}_2^{2+}$  solution was added into  $1\text{M NaOH}$  solution containing  $0.05\text{M}\sim 3.0\text{M}$  of  $\text{SiO}_2$  as an amorphous, silica gel. Less than  $2.5\text{M SiO}_2$  was totally dissolved in the  $1\text{M NaOH}$  solution. The pH decreased from 13.5 to 11.0 as the total amount of  $\text{SiO}_2$  increased to  $3.0\text{M}$ . In the sample with  $3.0\text{M SiO}_2$ , there was a white solid residue consisting of undissolved  $\text{SiO}_2$ . Fig. 14 shows changes in dissolved U concentration with different concentrations of dissolved Si. When the Si concentration is lower than  $0.5\text{M}$ , dissolved U concentration was low. The  $\text{UO}_2^{2+}$  precipitated out of the solution in the form of  $\text{Na}_2\text{U}_2\text{O}_7$  (confirmed by XRD). Samples with  $1.0\sim 1.5\text{M}$  dissolved Si had particulate-free solutions and the U concentration was high as  $0.21\sim 0.23\text{ mM}$ . At a dissolved Si concentration of  $2.0\text{M}$  (total Si =  $3\text{M}$ ), the dissolved U concentration decreased. This was probably due to  $\text{UO}_2^{2+}$  adsorption on the undissolved  $\text{SiO}_2$  gel or formation of U-silicate solids. However, the latter could not be detected by powder XRD.

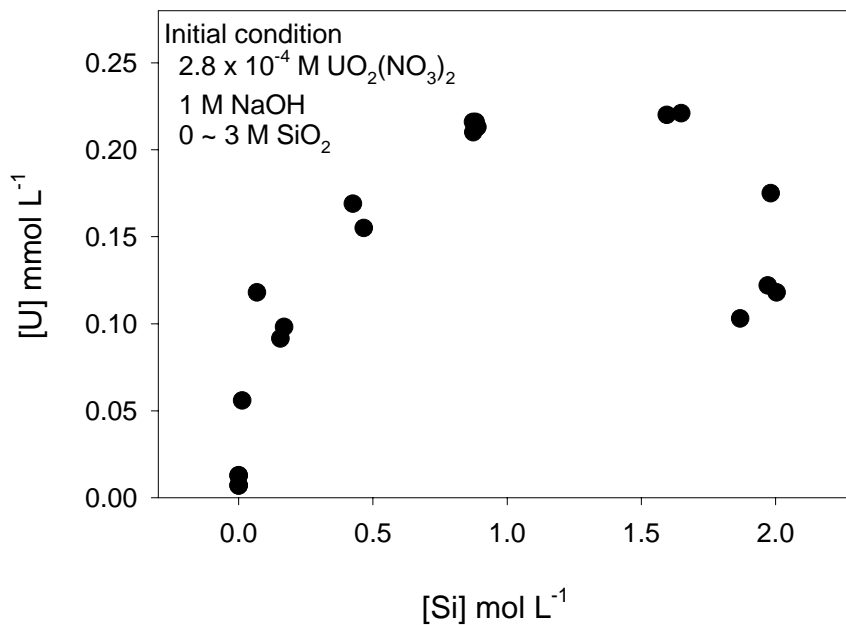


**Figure 14.** Changes in dissolved U concentration with Si concentration changes under 1M NaOH. pH decreased from 13.5 (at [Si]=0M) to 11.0 (at [Si] = 2.0M).

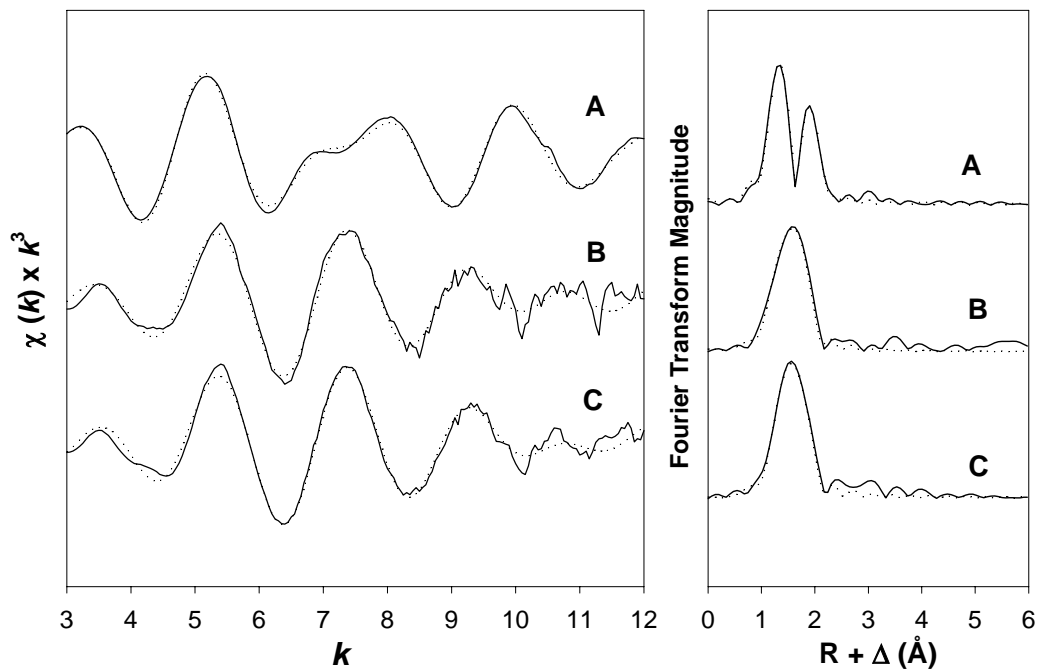


**Figure 15.** Uranium EXAFS spectra and corresponding Fourier Transforms for (A) 2.8mM  $\text{UO}_2(\text{NO}_3)_2$  stock solution (pH=4.2), (B) 0.28mM  $\text{UO}_2^{2+}$ , 1.0M  $\text{SiO}_2$ , and 1.0M NaOH, and (C)

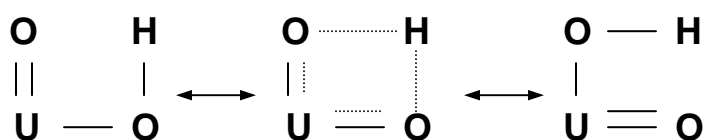
$[\text{UO}_2(\text{OH})_5]^{3-}$  prepared from 0.28mM  $\text{UO}_2(\text{NO}_3)_2$  and 1.0M TMA-OH. Solid lines are experimental data and dashed lines represent the fits.

**Table 2.** Summary of EXAFS results for (A) 2.8mM  $\text{UO}_2(\text{NO}_3)_2$  stock solution (pH=4.2), (B) 0.28mM  $\text{UO}_2^{2+}$ , 1.0M  $\text{SiO}_2$ , and 1.0M NaOH, and (C)  $[\text{UO}_2(\text{OH})_5]^{3-}$  prepared from 0.28mM  $\text{UO}_2(\text{NO}_3)_2$  and 1.0M TMA-OH.

Sample	Scattering path	N	R (Å)	$\sigma^2$	$E_0$
A. 2.8mM $\text{UO}_2(\text{NO}_3)_2$ stock solution	U-O <sub>ax</sub>	2.19	1.76	0.0020	-0.5
	U-O <sub>eq</sub>	5.17	2.41	0.0071	-0.5
B. 0.28mM $\text{UO}_2(\text{NO}_3)_2$ , 1M $\text{SiO}_2$ , 1M NaOH	U-O <sub>ax</sub>	2.40	1.79	0.0054	7.7
	U-O <sub>eq</sub>	5.17	2.23	0.0050	7.7
C. $[\text{UO}_2(\text{OH})_5]^{3-}$ from 0.28mM $\text{UO}_2(\text{NO}_3)_2$ and 1M TMA-OH	U-O <sub>ax</sub>	2.34	1.80	0.0037	10.4
	U-O <sub>eq</sub>	5.35	2.24	0.0052	10.4

Figure. 15 shows U EXAFS and corresponding RDFs for the 1M dissolved Si solution along with those for a  $\text{UO}_2(\text{NO}_3)_2$  stock solution (pH = 4) and uranyl hydroxide complexes,  $[\text{UO}_2(\text{OH})_5]^{3-}$  and  $[\text{UO}_2(\text{OH})_6]^{4-}$  that were prepared by adding  $\text{UO}_2^{2+}$  into 1.0M tetramethyl ammonium hydroxide (TMA-OH) after Wahlgren et al. (1999) and Clark et al. (1999). The summarized EXAFS results are shown in Table.2. The EXAFS results for  $\text{UO}_2(\text{NO}_3)_2$  stock solution (A) showed the structure of  $[\text{UO}_2(\text{H}_2\text{O})_5]^{2+}$ . Uranyl ion is known to exist as  $[\text{UO}_2(\text{H}_2\text{O})_5]^{2+}$  in acidic solutions (Wahlgren et al., 1999; Clark et al., 1999).

While the FT shows two peaks of U-O<sub>ax</sub> and U-O<sub>eq</sub> in  $\text{UO}_2(\text{NO}_3)_2$  stock solution, the peaks seem to be overlapped each other in samples B and C. There is no ligand exchange or electron delocalization in uranyl ion in acidic and neutral solution. In alkaline solutions, rapid oxo ligand exchange in the uranyl ion results in stretching of the axial U=O bonds and shortening of the equatorial U-O bond. As a result, the peaks of U-O<sub>ax</sub> and U-O<sub>eq</sub> in the sample B and C are overlapped.



There were no any other detectable scattering path besides U-O<sub>ax</sub> and U-O<sub>eq</sub>, suggesting no interaction between dissolved uranyl ion and dissolve silica. Sample B and C show almost identical EXAFS and FTs, and thus in coordination numbers (N) and bond distances (R) implying the presence of [UO<sub>2</sub>(OH)<sub>5</sub>]<sup>3-</sup> in the solution containing 0.28mM UO<sub>2</sub><sup>2+</sup>, 1.0M SiO<sub>2</sub>, and 1.0M NaOH. The question then remains, why does dissolved Si enhance the solubility of clarkeite? The magnitude of the change can not be accounted for changes in ionic strength since even minor increases in dissolved Si significantly changed the total dissolved U. Pheeqc calculations suggest that the dominant effect may be the formation of Na-metasilicate solution complex.

It must be noted that these measurements were made in the absence of dissolved Al. In real systems, it is unlikely that the dissolved Si concentration would approach 1.0~2.0M. Rather, one expects the formation of alumino-silicate phases. Indeed, addition of 0.1M Al(NO<sub>3</sub>)<sub>3</sub> into the totally dissolved solution containing 2.8mM U(VI) and 1M SiO<sub>2</sub> rapidly produced an amorphous phase, probably an aluminum-silicate. Interestingly almost all U(VI) was removed from solution by the addition of the Al.

## CONCLUSIONS

Under very high pH and high Na concentration Na<sub>2</sub>U<sub>2</sub>O<sub>7</sub> formation proceeded. As long as the Na concentration was kept high, Na<sub>2</sub>U<sub>2</sub>O<sub>7</sub> formation was not affected by CO<sub>3</sub><sup>2-</sup> (as Na<sub>2</sub>CO<sub>3</sub>). However, U speciation calculations indicate that when the dissolved Na concentration is low, Na<sub>2</sub>U<sub>2</sub>O<sub>7</sub> could be dissolved and the dissolution would be enhanced by CO<sub>2</sub>. It is interesting to note that dissolved Na concentrations in excess of 10 mol L<sup>-1</sup> have been reported for the vadose-zone pore-waters beneath SX-108 (citation). Thus clarkeite may be an important U(VI) phase even in the presence of atmospheric CO<sub>2</sub>.

*Acknowledgements-* This research was supported by the U.S. Department of Energy, Environmental Management Science Program (# DE-FG07-99ER15010) involving Drs. C.C. Ainsworth, G.E. Brown, P.J. Grandinetti, and J.E. Szecsody. XAFS experiments were performed at the Stanford Synchrotron Radiation Laboratory. The authors would like to thank Drs. C. Begg, J.M. Bigham, C. Chen, J.W. Olesik, and S. Prasad for assistance in data collection and analysis.

## 1. REFERENCES

- Clark, D.L., Conradson, S.D., Donohoe, R.J., Keogh, D.W., Morris, D.E., Palmer, P.D., Rogers, R.D., and Tait, C. D. (1999) Chemical speciation of the uranyl ion under highly alkaline conditions. Synthesis, structures, and oxo ligand exchange dynamics. *Inorg. Chem.*, 38, 1456-1466.
- Finch, R.J. and Ewing, R.C. (1997) Clarkeite: new chemical and structural data. *Am. Mineral.* 82, 607-619.
- George G.N. and Pickering I.J. (2000) EXAFSPAK A suite of computer programs for analysis of X-ray absorption spectra. Stanford Synchrotron Radiation Laboratory.

- Murphy, R.J., Lenhart, J.J., and Honeyman, B.D. (1999) The sorption of thorium (IV) and uranium (VI) to hematite in the presence of natural organic matter. *Colloids and Surfaces A: Physicochem. Eng. Aspects*, 157, 47-62.
- Newville, M. (2001) IFEFFIT: interactive XAFS analysis and FEFF fitting. *J. Synchrotron Rad.* 8, 322-324.
- Sylwester E.R., Hudson E.A. and Allen P.G. (2000) The structure of uranium (VI) sorption complexes on silica, alumina, and montmorillonite. *Geochim. Cosmochim. Acta* 64, 2431-2438.
- Wahlgren, U., Moll, H., Grenthe, I., Schimmelpfenning, B., Maron, L., Vallet, V., and Gropen, O. (1999) Structure of uranium (VI) in strong alkaline solutions. A combined theoretical and experimental investigation. *J. Phys. Chem. A*, 103, 8257-8264.
- Waite, T.D., Davis, J.A., Payne, T.E., Waychunas, G.A., and Xu, N. (1994) Uranium (VI) adsorption on ferrihydrite: Application of a surface complexation model. *Geochim. Cosmochim. Acta*, 58, 5465-5478
- Yamamura, T., Kitamura, A., Fukui, A., Nishikawa, S., Yamamoto, T., and Moriyama, H. (1998) Solubility of U(VI) in Highly Basic Solutions. *Radiochim. Acta*, **83**, 139-146.

### III. Research Products

#### A. Presentations

- Catalano, J.G., Warner, J.A., Chen, C-C., Yamakawa, I., Newville, M., Sutton, S.R., Ainsworth, C.C., Zachara, J.M., Traina, S.J. and Brown, G.E., Jr. (2001) X-ray spectroscopic and fluorescence study of the speciation and distribution of chromium in Hanford S-SX Tank Farm core samples. *Oral presentation at the 222<sup>nd</sup> National Meeting of the American Chemical Society*, August 2001, Chicago, IL
- He, Y. and S.J. Traina. Cr(VI) reduction by biotite at high pH and high ionic strength. Presented at the 2001 American Chemical Society Annual meeting, Chicago, IL. August 25 - 30.
- Prasad, S., I. Yamakawa, P. Grandinetti, and Traina, S.J., NMR spectra of Na, Al and Si in high level waste tank simulants. Oral presentation at the 222<sup>nd</sup> National Meeting of the American Chemical Society, August 2001, Chicago, IL
- Traina, S.J. (2001) The geochemistry of the Hanford vadose zone: Reactions of Cr near-field to SX-108. Annual Users Meeting, Advance Photon Source, Argonne National Laboratory, Argonne, IL
- Traina, S.J., G.E. Brown, C.C. Ainsworth, J.E. Szecsody, and N.P. Qafoku. 2000. Immobilization of radionuclides in the Hanford vadose zone by incorporation in solid phases. FY2001 EMSP Vadose Zone principal Investigation Workshop, November 28-30. W.R. Wiley Environmental Molecular Sciences Laboratory, Pacific Northwest National Laboratory, Richland, WA.
- Traina, S.J., P. Grandinetti, I. Yamakawa, S. Prasad, Y. He, G.E. Brown, J.G. Catalano, J.A. Warner, C.C. Ainsworth, N.P. Qafoku, and J.E. Szecsody. 2001. Immobilization of radionuclides in the Hanford vadose zone by incorporation in solid phases. FY2002 EMSP Vadose Zone Principal Investigation Workshop, November 5-6. WR Wiley Environmental Molecular Sciences Laboratory, Pacific Northwest National Laboratory, Richland, WA.
- Warner, J.A., Catalano, J.G., Grolimund, D., Traina, S.J., Ainsworth, C.C. and Brown, G.E., Jr. (2000) Extreme geochemistry: strontium interactions in hyperalkaline systems. *Poster presentation at the Tenth Annual V.M. Goldschmidt Conference*, September 2000, Oxford, UK.
- Warner, J.A., J.G. Catalano, C-C. Chen, I. Yamakawa, M. Newville, S. Sutton, S. Traina and G. E. Brown, Jr., Speciation and mapping of chromium in Hanford core samples determined by x-ray absorption spectroscopy, *Invited Presentation, Department of Chemistry, University of Toronto*, April 20, 2001.
- Warner, J.A., J.G. Catalano, C-C. Chen, I. Yamakawa, M. Newville, S. Sutton, S. Traina and G. E. Brown, Jr., Speciation and mapping of chromium in Hanford core samples determined by x-ray absorption spectroscopy, *Invited Presentation, The Glenn T. Seaborg Center, Lawrence Berkeley National Laboratory*, April 6, 2001.
- Yamaka, I and S.J. Traina (2001) Homogeneous and heterogeneous precipitation of U(VI) in hyperalkaline Na-aluminate solutions and Hanford sediments. Oral presentation at the 222<sup>nd</sup> National Meeting of the American Chemical Society, August 2001, Chicago, IL

## B. Publications and Technical Reports

- Catalano, J.G., Warner, J.A., Chen, C.-C., Yamakawa, I., Newville, M., Sutton, S.R., Ainsworth, C.C., Zachara, J.M., Traina, S.J., and Brown, G.E., Jr. (2001) Speciation of Chromium in Hanford Tank Farm SX-108 and 41-09-39 Core Samples Determined by X-ray Absorption Spectroscopy. *S-SX FIR Appendix E: Digest of S&T Evaluations*. United States Department of Energy, Richland Operations, Richland, WA 99352.
- He, Yongtian. 2003. Chromate reduction and immobilization under high pH and high ionic strength conditions. Ph.D. dissertation. The Ohio State University.
- He, Yongtian, Chia-chen Chen and S.J. Traina. Biotite dissolution and homogeneous reduction of Cr(VI) in hyperalkaline solutions *In Review Environ. Sci. Technol.*
- He, Yongtian, Bigham, J. and S.J. Traina. *In Preparation* Biotite dissolution and Cr(VI) reduction at elevated pH and ionic strengths. *Clays and Clay Minerals*.
- He, Yongtian, Bigham, J. and S.J. Traina. *In Preparation* Magnetite dissolution and Cr(VI) reduction at elevated pH and ionic strengths. *Clays and Clay Minerals*.
- He, Yongtian, Bigham, J. and S.J. Traina. *In Preparation* Magnetite conversion to goethite at elevated pH and ionic strength. *Geochim. Cosmochim. Acta*
- He, Yongtian, Bigham, J. and S.J. Traina. *In Preparation* Effects of high pH and ionic strength on Cr(VI) by Hanford sediments. *Environ. Sci. Technol.*
- Yamakawa, I. and S.J. Traina. Clarkeite formation in model mineral systems and Hanford sediments reacted with simulated high level waste fluids (submitted to *Geochem. Cosmochim. Acta.*, 2004).
- Zachara, J.M., J.G. Catalano, G.E. Brown, Jr., C.C. Ainsworth, S.J. Traina, J.P. McKinley, O. Oafoku, J.E. Szecsody, S.C. Smith, and J.A. Warner. 2004. Chromium speciation and mobility in a high level nuclear waste vadose zone plume. *Geochim. Cosmochim. Acta.* 68:13-30.